# A Novel Control Method for Transformerless H-Bridge Cascaded STATCOM With Star Configuration

Rong Xu, Yong Yu, Rongfeng Yang, Gaolin Wang, *Member, IEEE*, Dianguo Xu, *Senior Member, IEEE*, Binbin Li, and Shunke Sui

***Abstract*—This paper presents a transformerless static synchronous compensator (STATCOM) system based on multilevel H-bridge converter with star configuration. This proposed control methods devote themselves not only to the current loop control but also to the dc capacitor voltage control. With regards to the current loop control, a nonlinear controller based on the passivity-based control (PBC) theory is used in this cascaded structure STATCOM for the first time. As to the dc capacitor voltage control, overall voltage control is realized by adopting a proportional resonant controller. Clustered balancing control is obtained by using an active disturbances rejection controller. Individual balancing control is achieved by shifting the modulation wave vertically which can be easily implemented in a field-programmable gate array. Two actual H-bridge cascaded STATCOMs rated at 10 kV 2 MVA are constructed and a series of verification tests are executed. The experimental results prove that H-bridge cascaded STATCOM with the proposed control methods has excellent dynamic performance and strong robustness. The dc capacitor voltage can be maintained at the given value effectively.**

***Index Terms*—Active disturbances rejection controller (ADRC), H-bridge cascaded, passivity-based control (PBC), proportional resonant (PR) controller, shifting modulation wave, static synchronous compensator (STATCOM).**

## I. Introduction

FLEXIBLE ac transmission systems (FACTS) are being increasingly used in power system to enhance the system utilization, power transfer capacity as well as the power quality of ac system interconnections [1], [2]. As a typical shunt FACTS device, static synchronous compensator (STATCOM) is utilized at the point of common connection (PCC) to absorb or inject the required reactive power, through which the voltage quality of PCC is improved [3]. In recent years, many topologies have been applied to the STATCOM. Among these different types of topology, H-bridge cascaded STATCOM has been widely accepted in high-power applications for the following advantages: quick response speed, small volume, high efficiency, minimal interaction with the supply grid and its individual phase control ability [4]–[7]. Compared with a diode-clamped converter or flying capacitor converter, H-bridge cascaded STATCOM can obtain a high number of levels more easily and can be connected to the grid directly without the bulky transformer. This enables us to reduce cost and improve performance of H-bridge cascaded STATCOM [8].

There are two technical challenges which exist in H-bridge cascaded STATCOM to date. First, the control method for the current loop is an important factor influencing the compensation performance. However, many nonideal factors, such as the limited bandwidth of the output current loop, the time delay induced by the signal detecting circuit, and the reference command current generation process, will deteriorate the compensation effect. Second, H-bridge cascaded STATCOM is a complicated system with many H-bridge cells in each phase, so the dc capacitor voltage imbalance issue which caused by different active power losses among the cells, different switching patterns for different cells, parameter variations of active and passive components inside cells will influence the reliability of the system and even lead to the collapse of the system. Hence, lots of researches have focused on seeking the solutions to these problems.

In terms of current loop control, the majority of approaches involve the traditional linear control method, in which the nonlinear equations of the STATCOM model are linearized with a specific equilibrium. The most widely used linear control schemes are PI controllers [9], [10]. In [9], to regulate reactive power, only a simple PI controller is carried out. In [10], through a decoupled control strategy, the PI controller is employed in a synchronous $d$–$q$ frame. However, it is hard to find the suitable parameters for designing the PI controller and the performance of the PI controller might degrade with the external disturbance. Thus, a number of intelligent methods have been proposed to adapt the PI controller gains such as particle swarm optimization [11], neural networks [12], and artificial immunity [13]. In literature [14], [15], adaptive control and linear robust control have been reported for their antiexternal disturbance ability. In literature [16], [17], a popular dead-beat current controller is used. This control method has the high bandwidth and the fast reference current tracking speed. The steady-state performance of H-bridge cascaded STATCOM is improved, but

Manuscript received January 15, 2014; revised March 27, 2014; accepted April 18, 2014. Date of publication April 25, 2014; date of current version October 15, 2014. This work was supported by the National Natural Science Foundation of China (51237002) and by grants from the Power Electronics Science and Education Development Program of Delta Environmental and Educational Foundation (DREM2012001). Recommended for publication by Associate Editor F. Gao.

The authors are with the School of Electrical Engineering and Automation, Harbin Institute of Technology, Harbin 150001, China (e-mail: xurong0707@sina.com; yuyong@hit.edu.cn; yrf@hit.edu.cn; WGL818@hit.edu.cn; xudiang@hit.edu.cn; libinbinhit@126.com; suishunke@126.com).

Color versions of one or more of the figures in this paper are available online at http://ieeexplore.ieee.org.

Digital Object Identifier 10.1109/TPEL.2014.2320251

the dynamic performance is not improved. In [18], a dc injection elimination method called IDCF is proposed to build an extra feedback loop for the dc component of the output current. It can improve the output current qulity of STATCOM. However, the circuit configuration of the cascaded STATCOM is the delta configuration, but not the star configuration. Moreover, an adaptive theory-based improved linear sinusoidal tracer control method is proposed in [19] and a leaky least mean square-based control method is proposed in [20]. But these methods are not for STATCOM with the cascaded structure. By using the traditional linear control method, the controller is characterized by its simple control structure and parameter design convenience, but poor dynamic control stability.

Other control approaches apply nonlinear control which directly compensate for the system nonlinearities without requiring a linear approximation. In [21], an input–output feedback linearization controller is designed. By adding a damping term, the oscillation amplitude of the internal dynamics can be effectively decreased. However, the stability cannot be guaranteed [22]. Then, many new modified damping controllers are designed to enhance the stability and performance of the internal dynamics [23]–[26]. However, the implementation of these controllers is very complex. To enhance robustness and simplify the controller design, a passivity-based controller (PBC) based on error dynamics is proposed for STATCOM [27]–[30]. Furthermore, the exponential stability of system equilibrium point is guaranteed. Nevertheless, these methods are not designed on the basis of STATCOM with the H-bridge cascaded structure and there are no experimental verifications in these literatures.

In terms of dc capacitor voltage balancing control, there are three pivotal issues: overall voltage control, clustered balancing control, and individual balancing control. In literature [31], under the asumption of all dc capacitors being equally charged and balanced, they can only eliminate the imbalances caused by the inconsistent drive pulses without detecting all dc capacitor voltages. In [32]–[34], additional hardware circuits are required in the methods based on ac bus energy exchange and dc bus energy exchange, which will increase the cost and the complexity of the system. In [35], a method based on zero-sequence voltage injection is proposed and it will increase the dc capacitor voltage endurance capacity. On the contrary, the method using negative-sequence current in [36] does not need the wide margin of dc capacitor voltage, but the function of STATCOM is limited. In [8], the active power of the individual phase cluster is controlled independently, while the circuit condition is considered to be limited in practical use. In [37] and [38], a cosine component of the system voltage is superposed to the clustered output voltage, but it is easy to be affected by an inacurate phase-locked loop (PLL). In [39], the active voltage vector superposition method is proposed. However, the simulated and experimental results do not show the differences in control area and voltage ripple. The selective harmonic elimination modulation method is used in [40] and [41], in which dc voltage balancing control and low-frequency modulation are achieved. Compared with the method in [40] and [41], a method changing the phase-shift angle for dc voltage balancing control is proposed in [42] and [43], through which the desirable effect can be easily achieved, whereas it is limited by the capacity of STATCOM. In [44], the dc voltage and reactive power are controlled. However, it cannot be widely used due to fact that many nonideal factors are neglected. In [45] and [46], the proposed method assumes that all cells are distributed with equal reactive power and it uses the cosine value of the current phase angle. It could lead to system instability, when using the zero-crossing point of the cosine value. In [47] and [48], the results of experiments are obtained in the downscaled laboratory system. Thus, they are not very persuasive in this condition.

In this paper, a new nonlinear control method based on PBC theory which can guarantee Lyapunov function dynamic stability is proposed to control the current loop. It performs satisfactorily to improve the steady and dynamic response. For dc capacitor voltage balancing control, by designing a proportional resonant (PR) controller for overall voltage control, the control effect is improved, compared with the traditional PI controller. Active disturbances rejection controller (ADRC) is first proposed by Han in his pioneer work [49], and widely employed in many engineering practices [50]–[53]; furthermore, it finds its new application in H-bridge cascaded STATCOM for clustered balancing control. It realizes the excellent dynamic compensation for the outside disturbance. By shifting the modulation wave vertically for individual balancing control, it is much easier to be realized in field-programmable gate array (FPGA) compared with existing methods. Two actual H-bridge cascaded STATCOMs rated at 10 kV 2 MVA are constructed and a series of verification tests are executed. The experimental results have verified the viability and effectiveness of the proposed control methods.

## II. Configuration of the 10 kV 2 MVA STATCOM System

Fig. 1 shows the circuit configuration of the 10 kV 2 MVA star-configured STATCOM cascading 12 H-bridge pulse width modulation (PWM) converters in each phase and it can be expanded easily according to the requirement. By controlling the current of STATCOM directly, it can absorb or provide the required reactive current to achieve the purpose of dynamic reactive current compensation. Finally, the power quality of the grid is improved and the grid offers the active current only.

The power switching devices working in ideal condition is assumed. $u_{sa}$, $u_{sb}$, and $u_{sc}$ are the three-phase voltage of grid. $u_a$, $u_b$, and $u_c$ are the three-phase voltage of STATCOM. $i_{sa}$, $i_{sb}$, and $i_{sc}$ are the three-phase current of grid. $i_a$, $i_b$, and $i_c$ are the three-phase current of STATCOM. $i_{la}$, $i_{lb}$, and $i_{lc}$ are the three-phase current of load. $U_{\rm dc}$ is the reference voltage of dc capacitor. $C$ is the dc capacitor. $L$ is the inductor. $R_s$ is the starting resistor.

Table I summarizes the circuit parameters. The cascade number of $N = 12$ is assigned to H-bridge cascaded STATCOM, resulting in 36 H-bridge cells in total. Every cell is equipped with nine isolated electrolytic capacitors which the capacitance is 5600 $\mu$F. The dc side has no external circuit and no power source except for the dc capacitor and the voltage sensor. In each cluster, an ac inductor supports the difference between the sinusoidal

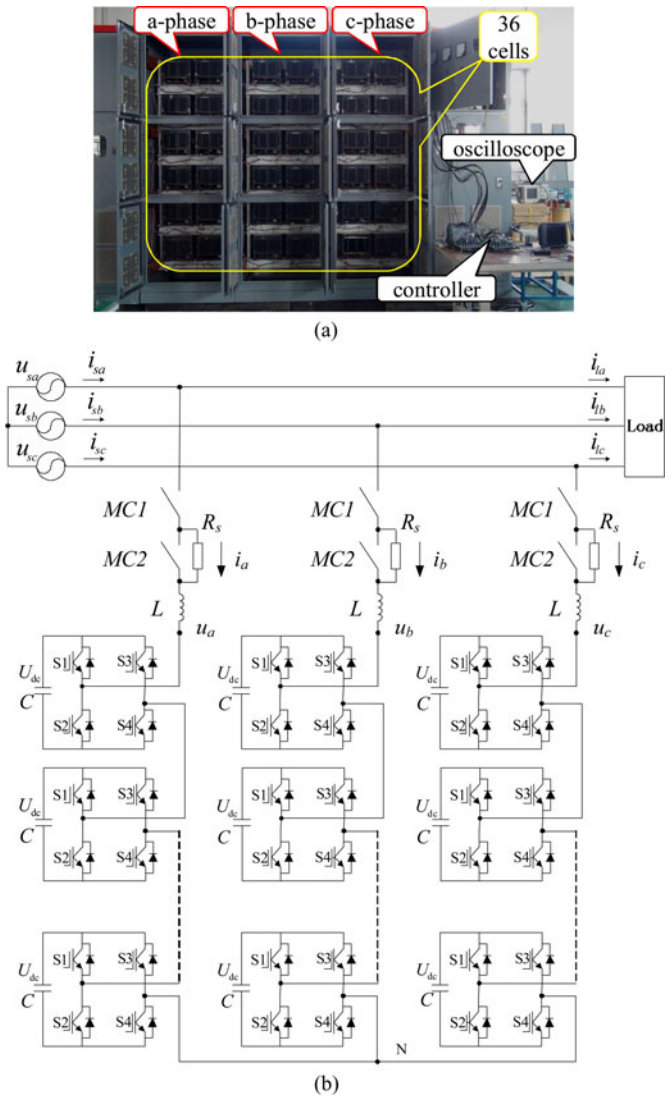


Fig. 1. Actual 10 kV 2 MVA H-bridge cascaded STATCOM. (a) Experimental hardware view. (b) Configuration of the experimental system.

voltage of the grid and the ac PWM voltage of STATCOM. The ac inductor also plays an important role in filtering out switch ripples caused by PWM. For selecting insulated-gate bipolar transistor (IGBT), considering the complexities of practical industrial fields, there might be the problems of the spike current and over load. Consequently, in order to ensure the stability and reliability of H-bridge cascaded STATCOM, and also improve the over load capability, the current rating of the selected IGBT should be reserved enough safety margin. In the proposed system, 1.4 times rated current operation is guaranteed, the peak current under the 1.4 times over load condition is 224 A, the additional 76 A $(30 - 224\ \text{A} = 76\ \text{A})$ is the safety margin of IGBT modules. Due to the previous considerations, the voltage and current ratings of IGBT which is selected as the switching element in main circuit are 1.7 kV and 300 A (Infineon EF300R17KE3).

The modulation technology adopts the carrier phase-shifted sinusoidal PWM (abbreviated as CPS-SPWM) with the carrier

TABLE I
CIRCUIT PARAMETERS OF THE EXPERIMENTAL SYSTEM

| | | |
|---|---|---|
| Grid voltage | $u_s$ | 10 kV |
| Rated reactive | $Q$ | 2 MVA |
| AC inductor | $L$ | 10 mH |
| Starting resistor | $R_s$ | 4 kΩ |
| DC capacitor capacitance | $C$ | 5600 μF |
| DC capacitor reference voltage | $U_{dc}$ | 800 V |
| Number of H-bridges | $N$ | 12 |
| PWM carrier frequency | $f$ | 1 kHz |

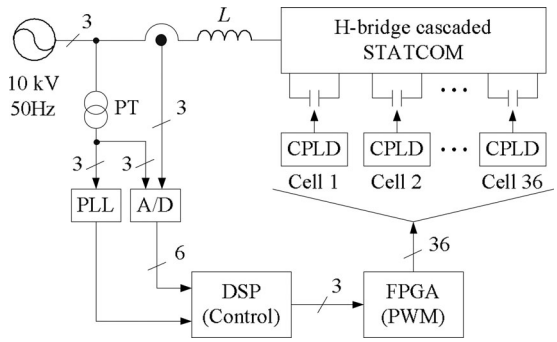


Fig. 2. Digital control system for 10 kV 2 MVA H-bridge cascaded STATCOM.

frequency of 1 kHz. Then, with a cascade number of $N = 12$, the ac voltage cascaded results in a 25-level waveform in line to neutral and a 49-level waveform in line to line. In each cluster, 12 carrier signals with the same frequency as 1 kHz are phase shifted by $2\pi/12$ from each other. When a carrier frequency is as low as 1 kHz, using the method of phase-shifted unipolar sinusoidal PWM, it can make an equivalent carrier frequency as high as 24 kHz. The lower carrier frequency can also reduce the switching losses to each cell.

As shown in Fig. 2, the main digital control block diagram of the 10 kV 2 MVA STATCOM experimental system consists of a digital signal processor (DSP) (Texas Instruments TMS320F28335), an FPGA (Altera CycloneIII EP3C25), and 36 complex programmable logic devices (CPLDs) (Altera MAXII EPM570). Most of the calculations, such as the detection of reactive current and the computation of reference voltage, are achieved by DSP. Then, DSP sends the reference voltages to the FPGA. The FPGA implements the modulation strategy and generates 36 PWM switching signals for each cell. CPLD of each cell receives PWM switching signal from the FPGA and drives IGBTs.

## III. CONTROL ALGORITHM

Fig. 3 shows a block diagram of the control algorithm for H-bridge cascaded STATCOM. The whole control algorithm mainly consists of four parts, namely, PBC, overall voltage control, clustered balancing control, and individual balancing

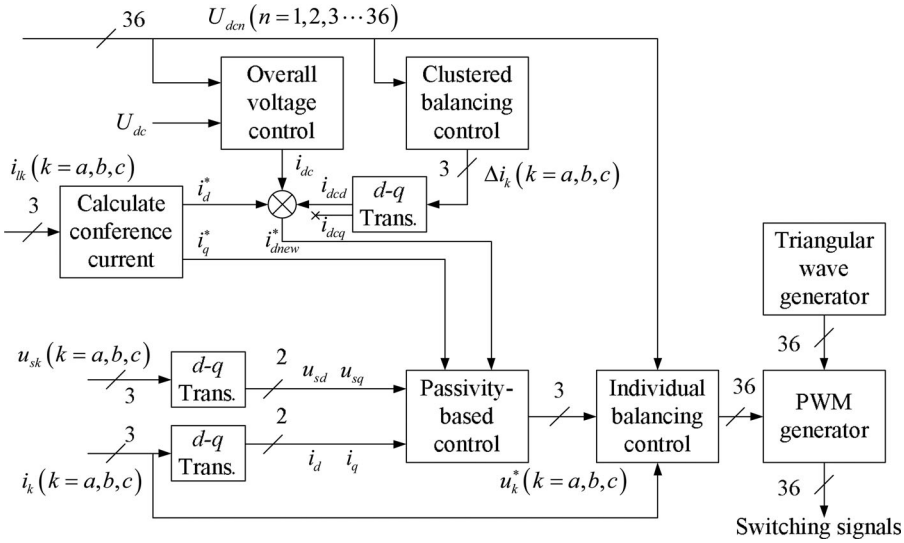


Fig. 3. Control block diagram for the 10 kV 2 MVA H-bridge cascaded STATCOM.

control. The first three parts are achieved in DSP, while the last part is achieved in the FPGA.

### A. PBC

Referring to Fig. 1, the following set of voltage and current equations can be derived:

$$\begin{cases} L\frac{di_a}{dt} = u_{sa} - u_a - Ri_a \\ L\frac{di_b}{dt} = u_{sb} - u_b - Ri_b \\ L\frac{di_c}{dt} = u_{sc} - u_c - Ri_c \end{cases} \tag{1}$$

where $R$ is the equivalent series resistance of the inductor. Applying the *d–q* transformations (1), the equations in *d–q* axis are obtained

$$\begin{cases} L\frac{di_d}{dt} = -Ri_d + \omega Li_q + u_{sd} - u_d \\ L\frac{di_q}{dt} = -\omega Li_d - Ri_q + u_{sq} - u_q \end{cases} \tag{2}$$

where $u_d$ and $u_q$ are the $d$-axis and $q$-axis components corresponding to the three-phase STATCOM cluster voltages $u_a, u_b$, and $u_c$. $u_{sd}$ and $u_{sq}$ are those corresponding to the three-phase grid voltages $u_{sa}, u_{sb}$, and $u_{sc}$. When the grid voltages are sinusoidal and balanced, $u_{sq}$ is always 0 because of $u_{sa}$ is aligned with the $d$-axis. $i_d$ and $i_q$ are the $d$-axis and $q$-axis components corresponding to the three-phase STATCOM currents $i_a, i_b$, and $i_c$.

Equation (2) is written as the following form:

$$\begin{bmatrix} L & 0 \\ 0 & L \end{bmatrix} \begin{bmatrix} \frac{di_d}{dt} \\ \frac{di_q}{dt} \end{bmatrix} + \begin{bmatrix} 0 & -\omega L \\ \omega L & 0 \end{bmatrix} \begin{bmatrix} i_d \\ i_q \end{bmatrix} + \begin{bmatrix} R & 0 \\ 0 & R \end{bmatrix} \begin{bmatrix} i_d \\ i_q \end{bmatrix} = \begin{bmatrix} u_{sd} - u_d \\ u_{sq} - u_q \end{bmatrix}. \tag{3}$$

To apply the PBC method, (3) is transformed into the form of the EL system model in this paper. EL system model is an important part of the nonlinear PBC theory and an effective modeling technology. It defines the energy equation by setting the general variable and harnesses the known theorem that can be used to analyze the dynamic performance to deduce the dynamic equations. This can make the system move along the minimize trajectory of Lagrangian integral [54]. EL system model could describe the characteristics of the system which is difficult to be disposed by linearization control method. This is the most important reason to use the EL system model for defining control system of H-bridge cascaded STATCOM.

Referring to [54], along with selecting $i_d$ and $i_q$ as state variables, it gives the following EL system model of (3):

$$\mathbf{M}\dot{\mathbf{x}} + \mathbf{J}\mathbf{x} + \mathbf{R}\mathbf{x} = \mathbf{u} \tag{4}$$

where $\mathrm{x} = \begin{bmatrix} i_d \\ i_q \end{bmatrix}$ is the state variable. $\mathbf{M} = \begin{bmatrix} L & 0 \\ 0 & L \end{bmatrix}$ is the positive definite inertial matrix and $\mathbf{M} = \mathbf{M}^{\mathrm{T}}$. $\mathrm{J} = \begin{bmatrix} 0 & -\omega L \\ \omega L & 0 \end{bmatrix}$ is the dissymmetry interconnection matrix and $\mathbf{J} = -\mathbf{J}^{\mathrm{T}}$. $\mathrm{R} = \begin{bmatrix} R & 0 \\ 0 & R \end{bmatrix}$ is the positive definite symmetric matrix which reflects the dissipation characteristic of the system. $\mathbf{u} = \begin{bmatrix} u_{sd} & -u_d \\ u_{sq} & -u_q \end{bmatrix}$ is the external input matrix which reflects the energy exchange between the system and environment.

As to a system, if there is positive semidefinite energy storage function $V(\mathbf{x})$ and positive definite function $Q(\mathbf{x})$, in the condition of $\forall\, T > 0$, the dissipative inequality (5) is true with the input $\boldsymbol{u}$ of the system, the output $\boldsymbol{y}$ of the system, and the energy supply rate $\mathbf{u}^{\mathrm{T}}\mathbf{y}$. This system is strictly passive. $\mathbf{u}^{\mathrm{T}}\mathbf{y}$ can be defined as the rate of energy supply along with the input $\mathbf{u}$ injected into the system from the external. $V$ is the energy storage function of the system

$$\dot{\mathbf{V}} \le \mathbf{u}^{\mathrm{T}}\mathbf{y} - \mathbf{Q}(\mathbf{x}). \tag{5}$$

For the strict passive system, if there is smooth and differentiable positive-definite energy storage function, $\mathrm{x} = 0$ is the

asymptotically stable equilibrium point for this system. Then, the storage function can be written as Lyapunov function.

Assume the energy storage function as (6) for H-bridge cascaded STATCOM

$$V = \frac{1}{2}\mathbf{x}^T\mathbf{M}\mathbf{x} = \frac{1}{2}L\left(i_d^2 + i_q^2\right). \tag{6}$$

By taking the derivative of $V$ and utilizing antisymmetric characteristic of $\mathbf{J}$, (7) is obtained as follows:

$$\dot{\mathbf{V}} = \mathbf{x}^{\mathrm{T}}\mathbf{M}\dot{\mathbf{x}} = \mathbf{x}^{\mathrm{T}}\left(\mathbf{u} - \mathbf{J}\mathbf{x} - \mathbf{R}\mathbf{x}\right) = \mathbf{x}^{\mathrm{T}}\mathbf{u} - \mathbf{x}^{\mathrm{T}}\mathbf{R}\mathbf{x}. \tag{7}$$

Setting $\mathbf{y} = \mathbf{x}$ and $Q(\mathbf{x}) = \mathbf{x}^{\mathrm{T}}\mathbf{R}\mathbf{x}$, the forms of (7) and (5) are the same. Thus, H-bridge cascaded STATCOM is the strictly passive. The controller can be designed for H-bridge cascaded STATCOM with the passivity theory.

When H-bridge cascaded STATCOM works in the steady conditions, because of the switching loss, the equivalent resistance loss and the loss of the capacitor itself, it will lead to a decline of the dc capacitor voltage. Thus, it needs to maintain dc capacitor voltage at the given value while compensating the reactive current for grid. And it has three expected stable equilibrium points: $U_{\mathrm{dc}}$ is the dc capacitor reference voltage. $i_d^*$ is the reference current of the $d$-axis. $i_q^*$ is the reference current of the $q$-axis.

Generally, the dc capacitor voltage of H-bridge cascaded STATCOM is maintained at the given value through absorbing the active current from the grid that can be achieved by controlling the $d$-axis active current. This $d$-axis *active current* $i_{\mathrm{dc}}^* = i_{\mathrm{dc}} + i_{\mathrm{d}cd}$ (as shown in Fig. 3) can be added to the $d$-axis reference current. The newfound $d$-axis reference current is $i_{d\mathrm{new}}^* = i_d^* + i_{\mathrm{dc}}^*$. Now, the three expected stable equilibrium points of the system can be revised two: $x_1^* = i_{d\mathrm{new}}^*$ and $x_2^* = i_q^*$.

Error system is established as follows:

$$\mathbf{x}_e = \mathbf{x} - \mathbf{x}^* = \begin{bmatrix} i_d - i_{d\mathrm{new}}^* & i_q - i_q^* \end{bmatrix}^T \tag{8}$$

where $\mathbf{x}^*$ is the expected stable equilibrium point of the system.

Substituting (8) into (4), the error dynamic equation of the system can be obtained as follows:

$$\mathbf{M}\left(\dot{\mathbf{x}}_e + \dot{\mathbf{x}}^*\right) + \mathbf{J}\left(\mathbf{x}_e + \mathbf{x}^*\right) + \mathbf{R}\left(\mathbf{x}_e + \mathbf{x}^*\right) = \mathbf{u} \tag{9}$$

that is

$$\mathbf{M}\dot{\mathbf{x}}_e + \mathbf{J}\mathbf{x}_e + \mathbf{R}\mathbf{x}_e = \mathbf{u} - (\mathbf{M}\dot{\mathbf{x}}^* + \mathbf{J}\mathbf{x}^* + \mathbf{R}\mathbf{x}^*). \tag{10}$$

To improve the speed of the convergence, from $\mathbf{x}$ to $\mathbf{x}^*$, and make error energy function reach zero, (10) is injected with damping. It can accelerate energy dissipation of the system and make the system converge the expected stable equilibrium point. The injected damping dissipation term as follows:

$$\mathbf{R}_d\mathbf{x}_e = \left(\mathbf{R} + \mathbf{R}_a\right)\mathbf{x}_e \tag{11}$$

where $\mathbf{R_d}$ is the damping matrix of the system. $\mathbf{R}_a = \begin{bmatrix} R_{a1} & 0 \\ 0 & R_{a2} \end{bmatrix}$ is the injected positive definite damping matrix and $R_{a1} > 0, R_{a2} > 0$.

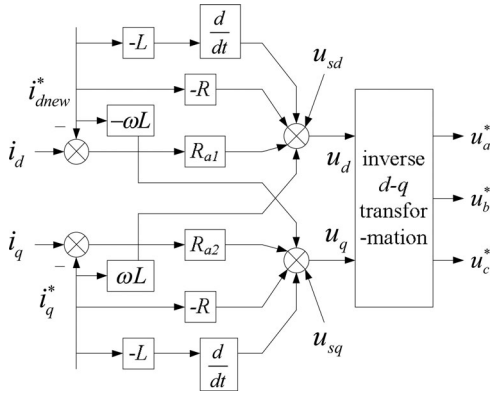


Fig. 4. Block diagram of PBC.

Substituting (11) into (10), the new error dynamic equation of the system can be achieved as follows:

$$\mathbf{M}\dot{\mathbf{x}}_e + \mathbf{J}\mathbf{x}_e + \mathbf{R}_d\mathbf{x}_e = \mathbf{u} - (\mathbf{M}\dot{\mathbf{x}}^* + \mathbf{J}\mathbf{x}^* + \mathbf{R}\mathbf{x}^* - \mathbf{R}_a\mathbf{x}_e) = \mathbf{x}\mathbf{i}. \tag{12}$$

The Lyapunov function of the system is obtained as

$$V_1 = \frac{1}{2}\mathbf{x}_e^T\mathbf{M}\mathbf{x}_e = \frac{1}{2}L\left(i_{\mathrm{ed}}^2 + i_{\mathrm{eq}}^2\right). \tag{13}$$

The derivative of (13) is achieved as

$$\dot{\mathbf{V}}_1 = \mathbf{x}_e^{\mathrm{T}}\mathbf{M}\dot{\mathbf{x}}\mathbf{e} = \mathbf{x}_e^T\left(\xi - \mathbf{J}\mathbf{x}_e - \mathbf{R}_d\mathbf{x}_e\right) = \mathbf{x}_e^T\xi - \mathbf{x}_e^{\mathrm{T}}\mathbf{R}_d\mathbf{x}_e. \tag{14}$$

As $\mathbf{M}$ is the positive-definite matrix, only if the disturbance $\boldsymbol{\xi} = \mathbf{0}$, (14) will be greater than zero. Thus, there must be a specific positive real number $\lambda$ that makes (15) true

$$\dot{\mathbf{V}}_1 = -\mathbf{x}_e^T\mathbf{R}_d\mathbf{x}_e \le -\lambda\mathbf{V}_1 < \mathbf{0}. \tag{15}$$

According to Lyapunov stability theorem, the system is exponential asymptotic stability.

For making $\boldsymbol{\xi} = \mathbf{0}$, the system needs to satisfy the condition as

$$\mathbf{M}\dot{\mathbf{x}}^* + \mathbf{J}\mathbf{x}^* + \mathbf{R}\mathbf{x}^* - \mathbf{R}_a\mathbf{x}_e = \mathbf{u}. \tag{16}$$

Based on (16), the passivity-based controller for H-bridge cascaded STATCOM can be obtained as

$$\begin{cases} u_d = -L\frac{di_{d\mathrm{new}}^*}{dt} + \omega L i_q^* - R i_{d\mathrm{new}}^* + R_{a1}\left(i_d - i_{d\mathrm{new}}^*\right) + u_{sd} \\ u_q = -L\frac{di_q^*}{dt} - \omega L i_{d\mathrm{new}}^* - R i_q^* + R_{a2}\left(i_q - i_q^*\right) + u_{sq}. \end{cases} \tag{17}$$

Fig. 4 shows a block diagram of the PBC and the three-phase command voltages $u_a^*, u_b^*$, and $u_c^*$ can be obtained by applying the inverse *d–q* transformation to $u_d$ and $u_q$.

### *B. Overall Voltage Control*

As the first-level control of the dc capacitor voltage balancing, the aim of the overall voltage control is to keep the dc mean voltage of all converter cells equalling to the dc capacitor reference voltage. The common approach is to adopt the conventional PI controller which is simple to implement. However, the output voltage and current of H-bridge cascaded STATCOM are the power frequency sinusoidal variables and the output power is

the double power frequency sinusoidal variable, it will make the dc capacitor also has the double power frequency ripple voltage. So, the reference current which is obtained in the process of the overall voltage control is not a standard dc variable and it also has the double power frequency alternating component and it will reduce the quality of STATCOM output current.

In general, when using PI controller, in order to ensure the stability and the dynamic performance of system, the bandwidth of voltage loop control is set to be 200–500 Hz and it is difficult to restrain the negative effect on the quality of STATCOM output current which is caused by the 100 Hz ripple voltage. Moreover, because of static error of PI controller, it will affect not only the first level control but also the second and the third one. Especially, during the startup process of STATCOM, it will make the voltage reach the target value with a much larger overshoot.

To resolve the problem, this paper adopts the PR controller for the overall voltage control. The gain of the PR controller is infinite at the fundamental frequency and very small at the other frequency. Consequently, the system can achieve the zero steady-state error at the fundamental frequency. By setting the cutoff frequency and the resonant frequency of the PR controller appropriately, it can reduce the part of ripple voltage in total error, decrease the reference current distortion which is caused by ripple voltage, and improve the quality of STATCOM output current. Moreover, the dynamic performance and the dynamic response speed of the system also can be improved. In particular, during the startup process of STATCOM, the much larger dc voltage overshoot can be restrained effectively.

The PR controller is composed of a proportional regulator and a resonant regulator. Its transfer function can be expressed as

$$G_{\mathrm{PR}}(s) = k_p + \frac{2k_r\omega_c s}{s^2 + 2\omega_c s + \omega_0^2} \tag{18}$$

where $k_p$ is the proportional gain coefficient. $k_r$ is the integral gain coefficient. $\omega_c$ is the cutoff frequency. $\omega_0$ is the resonant frequency. $k_r$ influences the gain of the controller but the bandwidth. With $k_r$ increasing, the amplitude at the resonant frequency is also increased and it plays a role in the elimination of the steady-state error. $\omega_c$ influences the gain of the controller and the bandwidth. With $\omega_c$ increasing, the gain and the bandwidth of the controller are both increased.

This paper selects $k_p = 0.05, k_r = 10, \omega_c = 3.14$ rad/s, and $\omega_0 = 100\pi$ as the controller parameters. Fig. 5 shows the bode plots of the PR controller with the previous parameters and Fig. 6 shows the block diagram of overall voltage control. The signal of voltage error is obtained by comparing the dc mean voltage of all converter cells with the dc capacitor reference voltage. Then, the signal of voltage error is regulated by the PR controller and delivered to the current loop as a part of the reference current. $U_{\mathrm{dc}}$ is the dc capacitor reference voltage. $U_{\mathrm{dc}}^*$ is the mean value of overall voltage. $i_{\mathrm{dc}}$ is the active control current for overall voltage control.

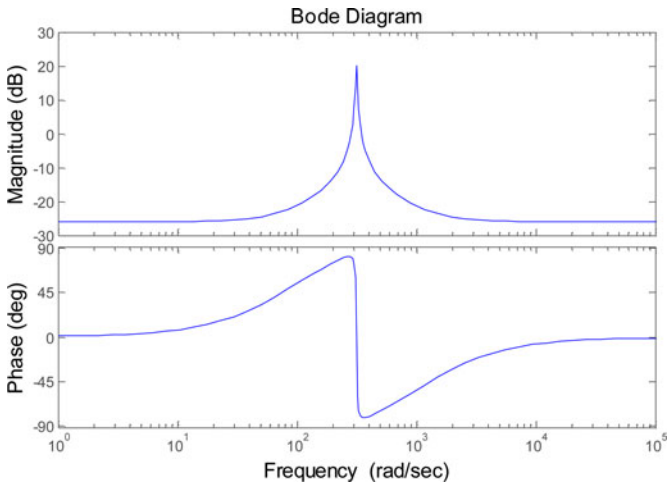


Fig. 5. Bode plots of the PR controller.

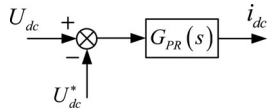


Fig. 6. Block diagram of overall voltage control.

### C. Clustered Balancing Control

Taking the clustered balancing control as the second level control of the dc capacitor voltage balancing, the purpose is to keep the dc mean voltage of 12 cascaded converter cells in each cluster equaling the dc mean voltage of the three clusters. ADRC is adopted to achieve it. Then, it requires several steps to complete the design of ADRC for H-bridge cascaded STATCOM, which are as follows.

1) According to (1), H-bridge cascaded STATCOM is a first-order system; thus, the first-order ADRC is designed. Taking the dc capacitor voltage of each cluster as the controlled object for analysis, the clustered balancing control model is built and the input and output variables and the controlled variable of the controlled object are determined.

2) By using the nonlinear tracking differentiator (TD) which is a component of ADRC, the transient process for the reference input of the controlled object is arranged and its differential signal is extracted.

Selecting the mean value of overall voltage $U_{\mathrm{dc}}^*$ as the reference voltage, TD is obtained via linear differential element and it can be expressed as

$$\dot{v}_1 = -r_1 fal\left[\left(v_1 - U_{\mathrm{dc}}^*\right), \alpha_1, \delta_1\right] \tag{19}$$

where $v_1$ is the tracking signal of reference voltage $U_{\mathrm{dc}}^*$ and $\dot{v}_1$ is the differential signal of the reference voltage $U_{\mathrm{dc}}^*$. $r_1$ is the speed tracking factor which reflects the changing rule of TD. The larger the $r_1$, the faster the tracking speed and the larger the overshoot. Thus, it needs to select $r_1$ properly according to the requirement of the actual system. $\alpha_1$ and $\delta_1$ are the adjustable control parameters. $\alpha_1$ determines the nonlinear form. The control

effect will be changed greatly with the appropriate $\alpha_1$. $\delta_1$ determines the size of the $fal$ function linear range.

3) With the extended state observer (ESO) in ADRC, the uncertainties and the disturbances which lead to the unbalancing of the clustered dc capacitor voltages are observed and estimated dynamically.

The second-order ESO designed for the dc capacitor voltage of STATCOM could be written as

$$\begin{cases} \xi = z_1 - U_{kdc} \\ \dot{z}_1 = z_2 - r_{21} fal\left(\xi, \alpha_2, \delta_2\right) + b\Delta i_k \\ \dot{z}_2 = -r_{22} fal\left(\xi, \alpha_2, \delta_2\right) \end{cases} \tag{20}$$

where the $fal$ function $fal\left(\xi, \alpha, \delta\right)$ is defined as

$$fal\left(\xi, \alpha, \delta\right) = \begin{cases} |\xi|^{\alpha} \, sign\left(\xi\right) & \left(|\xi| > \delta\right) \\ \xi / \delta^{1-\alpha} & \left(|\xi| \le \delta\right). \end{cases} \tag{21}$$

$U_{k\mathrm{dc}}$ $(k = a, b, c)$ is the real-time detected value of the dc mean voltage of 12 cascaded converter cells in each cluster in current cyclical and it is used as known parameter. $z_1$ is the state estimation signal of the dc capacitor voltage. $\xi$ is the control deviation of the system. $z_2$ is the internal and the external disturbance estimate signals of the controlled object. $\Delta i_k$ is the control variable. $b$ is the feedback coefficient of $\Delta i_k (k = a, b, c)$. $r_{21}, r_{22}, \alpha_2$, and $\delta_2$ are the adjustable control parameters. $r_{22}$ has an effect on the delay of $z_2$. The larger the $r_{22}$, the smaller the delay. But, the larger $r_{22}$ will lead to system oscillation. With $r_{21}$ increasing slightly, the system oscillation could be damped. However, it will result in system divergence. Consequently, the adjustment of $r_{21}$ and $r_{22}$ requires mutual coordination. It can set $r_{22}$ beforehand and then improve the control effect with increasing $r_{21}$ gradually.

Actually, there are errors in the detection unit of the dc capacitor voltage of STATCOM. Thus, control precision of the dc capacitor voltage can be improved considerably by using $z_1$ to estimate the state of the actual dc capacitor voltage precisely. For the changing of the system operation parameters in different applied environments, $z_2$ can estimate the unknown disturbances accurately and optimize the dynamic response speed of the clustered balancing control. Whether the unknown disturbances can be estimated accurately with ESO directly influences the control effect of ADRC. Therefore, the tuning of ESO parameters is very critical.

4) Nonlinear state error feedback (NLSEF) unit, a very important part of ADRC, is used to calculate the control variable of the active power adjustment for the clustered balancing control. However, in the practical application, the selection of NLSEF unit parameters in common ADRC is very difficult. Therefore, it is simplified with the linear optimization method in this paper and the newly obtained NLSEF unit can be expressed as

$$\begin{cases} \xi_1 = z_1 - v_1 \\ i_0 = r_3 fal\left(\xi_1, \alpha_3, \delta_3\right) \\ \Delta i_k = i_0 - z_2 / b \end{cases} \tag{22}$$

where $fal$ function is defined as (21). $\xi_1$ is the error value between the tracking signal $v_1$ and the state estimation signal $z_1$.

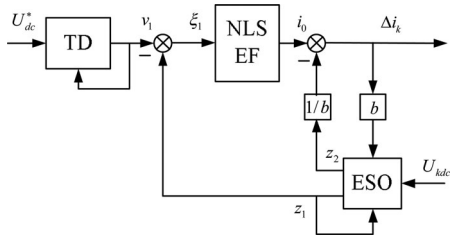


Fig. 7. Block diagram of clustered balancing control.

$i_0$ is the control variable without the disturbance feedback compensation. $b$ is the feedback coefficient which has relations with the control variable $\Delta i_k$ and the state variable of the ESO. If the controlled object existed delay, with a larger $b$, it would generate a large error control signal making the response speed of the output faster and compensation of the internal and the external disturbances more effective. $r_3, \alpha_3$, and $\delta_3$ are the adjustable control parameters. The regulating speed can be controlled by appropriately adjusting $r_3$. However, the faster regulating speed might cause increased overshoot and system oscillation.

5) Finally, by combining NLSEF unit with the observed disturbances from ESO, the simplified ADRC can be achieved and then the clustered balancing control of H-bridge cascaded STATCOM can be realized.

Fig. 7 shows a block diagram of the clustered balancing control with the simplified ADRC. When ADRC receives the reference voltage $U_{\mathrm{dc}}^*$ and the real-time detected value of the dc mean voltage $U_{k\mathrm{dc}}$ $(k = a, b, c)$ of 12 cascaded converter cells in each cluster, it will trace the reference voltage rapidly with TD and obtain the tracking signal $v_1$ by filtering. Then, by subtracting the tracking signal $v_1$ from the state estimation signal of the dc capacitor voltage $z_1$, the control deviation command $\xi_1$ of the system voltage is calculated. $\xi_1$ is used as the input signal of NLSEF. Finally, the active adjustment control current $\Delta i_k$ $(k = a, b, c)$ of the clustered balancing control is achieved by subtracting the disturbance estimate signals which obtained in ESO from the output result $i_0$ of NLSEF.

### *D. Individual Balancing Control*

As the overall dc voltage and the clustered dc voltage are controlled and maintained, the individual control becomes necessary because of the different cells have different losses. The aim of the individual balancing control as the third level control is to keep each of 12 dc voltages in the same cluster equalling to the dc mean voltage of the corresponding cluster. It plays an important role in balancing 12 dc mean capacitor voltages in each cluster. Due to the symmetry of structure and parameters among the three phases, a-phase cluster is taken as an example for the individual balancing control analysis.

Fig. 8 shows the charging and discharging states of one cell. According to the polarity of output voltage and current of the cell, the state of the dc capacitor can be judged. Then, the dc capacitor voltage will be adjusted based on the actual voltage value.

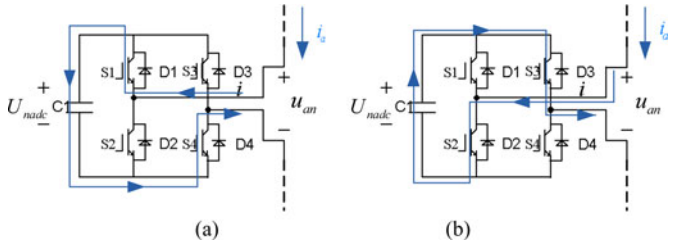


Fig. 8. Charging and discharging states of one cell. (a) Charging state. (b) Discharging state.

As shown in Fig. 8, at some point, the direction of the current is from the grid to STATCOM. If S1 and S4 are open, the output voltage of the $n$th cell is positive. The current flows into the dc capacitor along the direction which is shown in Fig. 8(a) and charges the capacitor. Likewise, if S2 and S3 are open, the output voltage of the $n$th cell is negative. The current flows into the dc capacitor along the direction which is shown in Fig. 8(b) and discharges the capacitor. Obviously, to make the capacitor voltage of each cell tend to be consistent, the turn-on time of the cell with the lower voltage should be extended and the turn-on time of the cell with the higher voltage should be shortened in charging state. Then, in discharging state, the process is contrary. The adjustment principle of the dc capacitor voltage can be summarized as follows.

1) When $(i_a \times u_{an}) > 0$, if $U_{nadc} < U_{adc}$, it needs to increase the duty cycle. If $U_{nadc} > U_{adc}$, it needs to reduce the duty cycle.
2) When $(i_a \times u_{an}) < 0$, if $U_{nadc} > U_{adc}$, it needs to increase the duty cycle. If $U_{nadc} < U_{adc}$, it needs to reduce the duty cycle.

$i_a$ is output current of a-phase cluster. $u_{an}$ is ac output voltage of the $n$th $(n = 1, 2, \cdots, 12)$ cell of a-phase cluster. $U_{adc}$ is the dc mean voltage of 12 cascaded converter cells in a-phase cluster. $U_{nadc}$ is the capacitor voltage of the $n$th cell of a-phase cluster.

According to the previous method, the direction and the magnitude of adjustment of the duty cycle for one cell can be achieved easily at some point.

Fig. 9 shows the adjustment method of the duty cycle by shifting the modulation wave vertically. Taking the first half period of the modulation wave as an example, the value of the modulation wave is greater than zero and the cell outputs zero level and 1 level. When the level is zero, the capacitor is not connected to the main circuit and it is not in the state of the charging and discharging. To reduce the charging time for one capacitor, it needs to reduce the action time of 1 level. And it can be realized by reducing the turn-on time of S1and S4 (as shown in Fig. 8). The state of the left bridge arm is decided by comparing the normal modulation wave with the triangular carrier. The state of the right bridge arm is decided by comparing the opposite modulation wave with the triangular carrier. Therefore, taking $x$-axis as the boundary, the duty cycle is reduced by shifting down the normal modulation wave and shifting up the opposite modulation wave according to

$$u_i = u_{i0} - k * e_{U\mathrm{dc}} \tag{23}$$

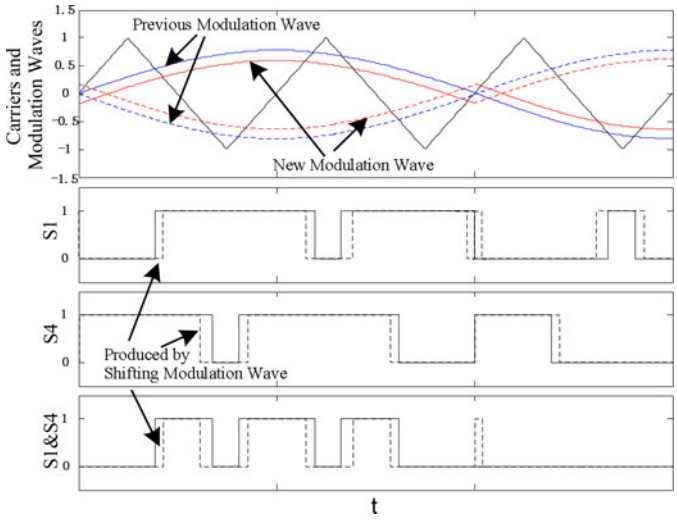


Fig. 9. Process of shifting modulation wave.

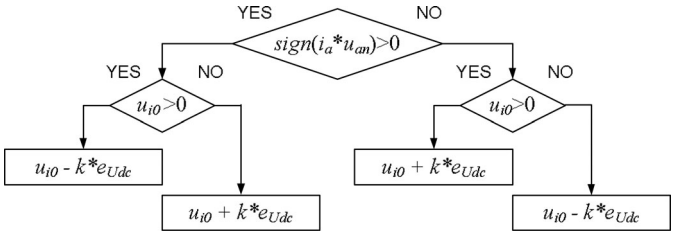


Fig. 10. Flowchart of shifting modulation wave.

$$u_i = u_{i0} + k * e_{U\mathrm{dc}} \tag{24}$$

where $e_{U\mathrm{dc}} = U_{nadc} - U_{adc}$. $k$ is regulation coefficient. $u_{i0}$ is the previous modulation wave. $u_i$ is the new modulation wave.

The previous principle is also suitable for reducing discharging time and prolonging the charging and discharging times of the cell. Summing up the previous analysis, the method can be illustrated as follows.

1) If the requirement is to reduce the duty cycle, it needs to shift down the normal modulation wave and shift up the opposite modulation wave.
2) If the requirement is to prolong the duty cycle, it needs to shift up the normal modulation wave and shift down the opposite modulation wave.

The value of shifting is decided by $k * e_{U\mathrm{dc}}$ and the flowchart is shown in Fig. 10.

The previous method is the modulation strategy that is based on CPS-SPWM in this paper and it is very easy to be realized in the FPGA. But, it is not to say that this method must be used like this only. In order to regulate the duty cycle, as long as the pulse signal is achieved by comparing the modulation wave with the carrier, the modulation strategy is able to use this method. The implementation block diagram of the individual balancing control method is shown in Fig. 11.

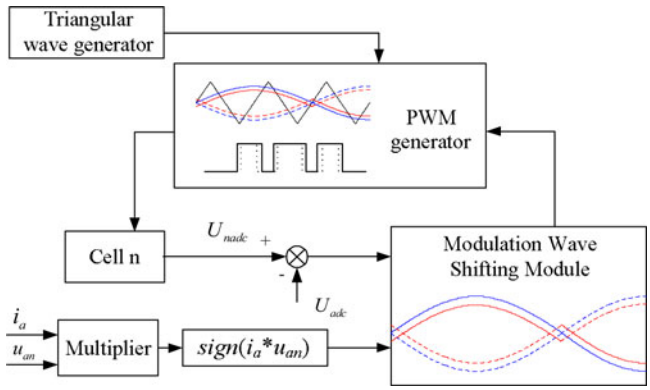


Fig. 11. Block diagram of individual balancing control.

## IV. Experimental Results

To verify the correctness and effectiveness of the proposed methods, the experimental platform is built according to the second part of this paper. Two H-bridge cascaded STATCOMs are running simultaneously. One generates the set reactive current and the other generates the compensating current that prevents the reactive current from flowing into the grid. The experiment is divided into two parts: the current loop control experiment and the dc capacitor voltage balancing control experiment. In current loop control experiment, the measured experimental waveform is the current of a-phase cluster and it is recorded by the oscilloscope. In dc capacitor voltage balancing control experiment, the value of dc capacitor voltages are transfered into DSP by a signal acquisition system and they can be recorded and observed by CCS software in computer. Finally, with the exported experimental data from CCS, experimental waveform is plotted by using MATLAB.

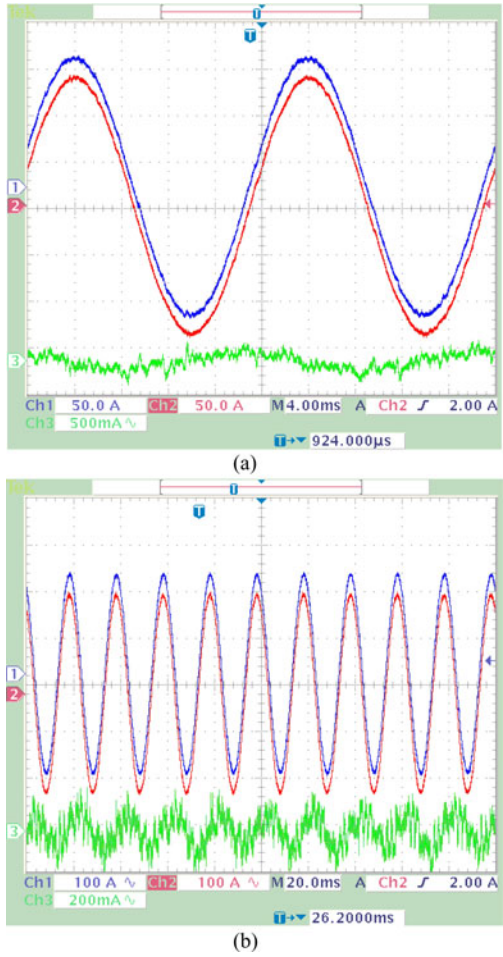


Fig. 12. Experimental results verify the effect of PBC in steady-state process. (a) Ch1: reactive current; Ch2: compensating current; Ch3: residual current of grid. (b) Ch1: reactive current; Ch2: compensating current; Ch3: residual current of grid.

### A. Current Loop Control Experiment

The current loop control experiment is divided into four processes: steady-state process, dynamic process, startup process, and stopping process.

Fig. 12 shows the experimental results verifying the effect of PBC in steady-state process. As shown in Fig. 12(a), it is the experimental result of the full load test. With the proposed control method, the reactive current is compensated effectively. The error of the compensation is very small. The residual current of the grid is also quite small.The phase of the compensating current is basically the same as the phase of the reactive current. The waveforms of the compensating current and the reactive current are smooth and they have the small distortion and the great sinusoidal shape. As shown in Fig. 12(b), it is the experimental result of the over load test. When STATCOM is running in over load state (about 1.4 times current rating), due to the selected IGBT has been reserved the enough safety margin, STATCOM still can run continuously and steadily. The over load capability of STATCOM is improved greatly and the operating reliability of STATCOM in practical industrial field is enhanced effectively. However, considering the over load capability of other devices in STATCOM and the capacity of STATCOM itself, STATCOM is not suggested for long-term operation in over load state.

Fig. 13 shows the dynamic performance of STATCOM in the dynamic process. When two STATCOMs are running in the steady-state process, at some point, the one generating the reactive current decreases output current suddenly. Meanwhile, the other one which generates the compensating current has the same mutative value. The residual current of the grid has a transient distortion and then returns to the steady state immediately. The dynamic response of STATCOM is very fast.

Fig. 14 shows the experimental results in the startup process and stopping process. As shown in Fig. 14(a), when STATCOM generating the reactive current starts running, the other STATCOM which generates the compensating current also starts running right away and generates the corresponding compensating current to compensate the reactive current. Similarly, in Fig. 14(b), when STATCOM which outputs the reactive current stops running, the other STATCOM which outputs the compensating current also stops running at once and there is no significant overcompensation. When the system starts running or stops running, the residual current of the grid has a very small

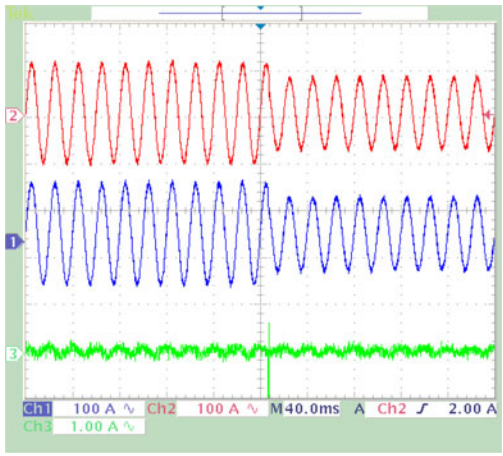


Fig. 13. Experimental results show the dynamic performance of STATCOM in the dynamic process. Ch1: reactive current; Ch2: compensating current; Ch3: residual current of grid.

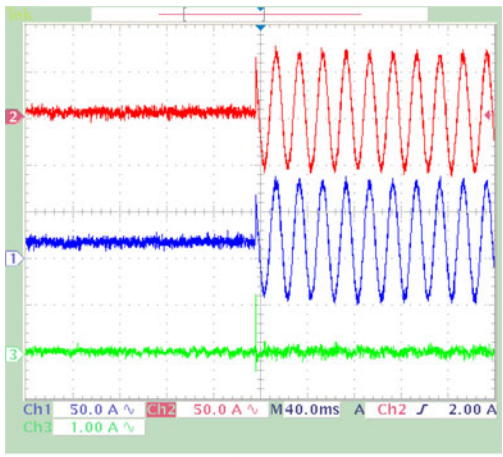


(a)

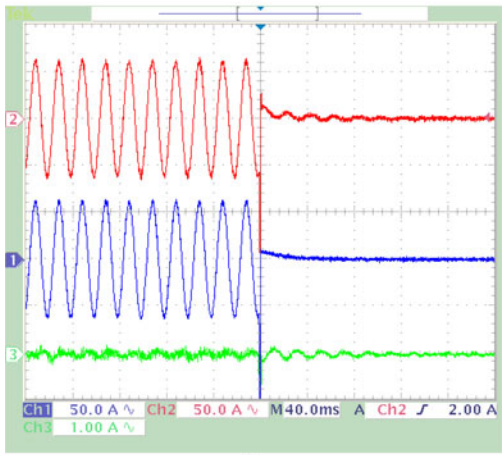


(b)

Fig. 14. Experimental results in the startup process and stopping process. (a) Ch1: reactive current; Ch2: compensating current; Ch3: residual current of grid. (b) Ch1: reactive current; Ch2: compensating current; Ch3: residual current of grid.

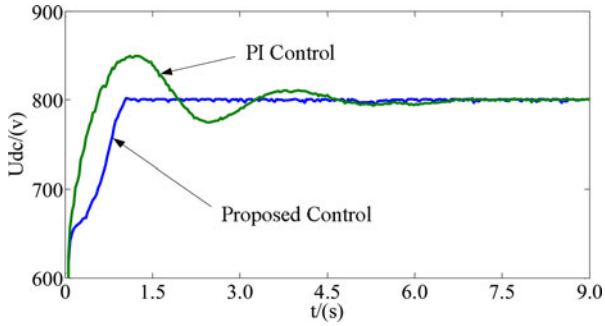


Fig. 15. Experimental waveforms for testing overall voltage control in the startup process.

instantaneous changewhile whole process is very quick and has no impact on the grid.

The results obtained earlier in the current loop control experiment show that STATCOM can track the reference command current accurately and compensate the reactive current rapidly when the reactive current changes suddenly by adopting the proposed control method. The compensation precision of STATCOM is high and the dynamic response of STATCOM is fast.

### *B. DC Capacitor Voltage Balancing Control Experiment*

STATCOM which generates the compensating current is taken as an example to verify the effect of dc capacitor voltage balancing control.

Fig. 15 shows the experimental waveforms for testing overall voltage control in the startup process. This paper selects $k_p = 0.05, k_r = 10, \omega_c = 3.14$ rad/s, and $\omega_0 = 100\pi$ as the PR controller parameters. $k_p = 0.5$ and $k_i = 0.01$ are selected as the PI controller parameters and the selecting rule is according to the method which is proposed by Hirofumi Akagi in literature [55]. The dc capacitor reference voltage $U_{\rm dc}$ is set at 800 V. The two lines denote the dc mean voltage of all converter cells $U^*_{\rm dc}$ with the PI control and the proposed control (PR control), respectively, and both exhibit good performance on tracking the voltage of the set point. The PI controller can make the voltage reach the target value rapidly, but it still requires roughly double the settling time with a much larger overshoot (greater than 6%) than that of the proposed controller. And the proposed controller provides a very smooth response. The proposed control method exhibits better performance in terms of response time and damping profile compared with the PI control.

Fig. 16 shows the experimental waveforms for testing clustered balancing control which is realized by ADRC in the startup process and dynamic process. As shown in Fig. 16(a), in the startup process, although all converter cells have different losses, the dc mean voltage $U_{k\rm dc}$ $(k = a, b, c)$ of 12 cascaded converter cells in each cluster can attain consistent with $U^*_{\rm dc}$ rapidly. The dc voltage deviation is no more than 10 V. After reaching steady state, $U_{k\rm dc}$ $(k = a, b, c)$ have less deviation compared with $U^*_{\rm dc}$ and the steady-state error is less than 5 V. In Fig. 16(b), when the output current of STATCOM has a sharp change, $U^*_{\rm dc}$ is maintained at the reference voltage value. But the waveforms of

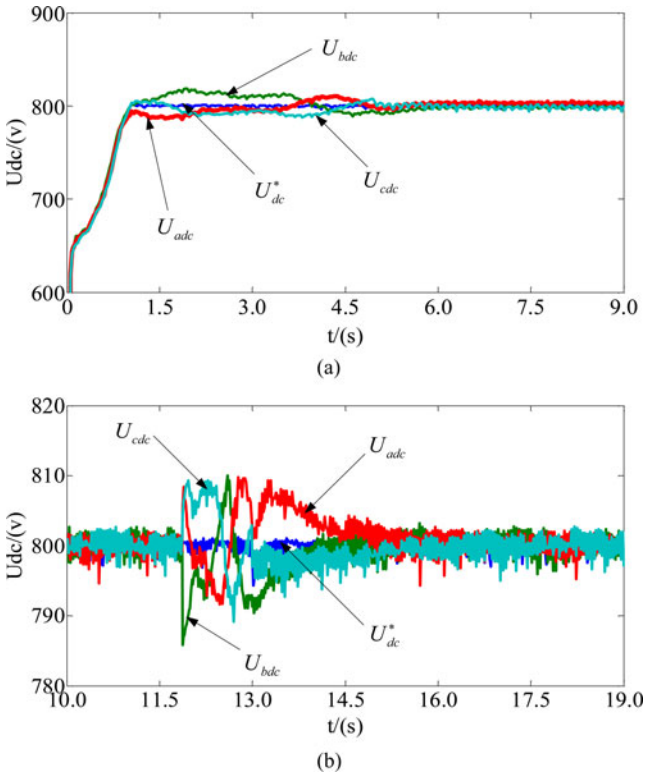


Fig. 16. Experimental waveforms for testing clustered balancing control in the startup process and dynamic process. (a) DC mean voltage of all converter cells $U_{\rm dc}^*$; dc mean voltage $U_{k\rm dc}$ $(k=a,b,c)$ of 12 cascaded converter cells in each cluster. (b) DC mean voltage of all converter cells $U_{\rm dc}^*$; dc mean voltage $U_{k\rm dc}$ $(k=a,b,c)$ of 12 cascaded converter cells in each cluster.

$U_{k\rm dc}$ $(k=a,b,c)$ are shown clearly as three different curves. Then, the clustered balancing control is triggered and the three curves converge as one quickly. $U_{k\rm dc}$ $(k=a,b,c)$ can still attain consistent with $U_{\rm dc}^*$. The max deviation is no more than 15 V and the steady-state error is less than 5 V. The results verify that the proposed method of clustered balancing control is effective for balancing dc voltages among three clusters. And it avoids the overvoltage protection of dc capacitor which can make STATCOM stop working.

Fig. 17 shows the experimental waveforms of 12 cells in a-phase cluster for testing individual balancing control which is realized by shifting the modulation wave vertically in steady-state process. The dc voltages of all cells are maintained at the given values (800 V) with the small voltage ripple. This experiment verifies that CPS-SPWM with the proposed method of individual voltage control is effective in regulating individual dc voltages.

Results of dc capacitor voltage balancing control show that the proposed control methods can coordinate with each other and achieve the best control effect. They also improve the steady state and dynamic performance of STATCOM.

## V. Conclusion

This paper has analyzed the fundamentals of STATCOM based on multilevel H-bridge converter with star configuration. And then, the actual H-bridge cascaded STATCOM rated at 10 kV 2 MVA is constructed and the novel control methods are also proposed in detail. The proposed methods has the following characteristics.

1) A PBC theory-based nonlinear controller is first used in STATCOM with this cascaded structure for the current loop control, and the viability is verified by the experimental results.
2) The PR controller is designed for overall voltage control and the experimental result proves that it has better performance in terms of response time and damping profile compared with the PI controller.
3) The ADRC is first used in H-bridge cascaded STATCOM for clustered balancing control and the experimental results verify that it can realize excellent dynamic compensation for the outside disturbance.
4) The individual balancing control method which is realized by shifting the modulation wave vertically can be easily implemented in the FPGA.

The experimental results have confirmed that the proposed methods are feasible and effective. In addition, the findings of this study can be extended to the control of any multilevel voltage source converter, especially those with H-bridge cascaded structure.

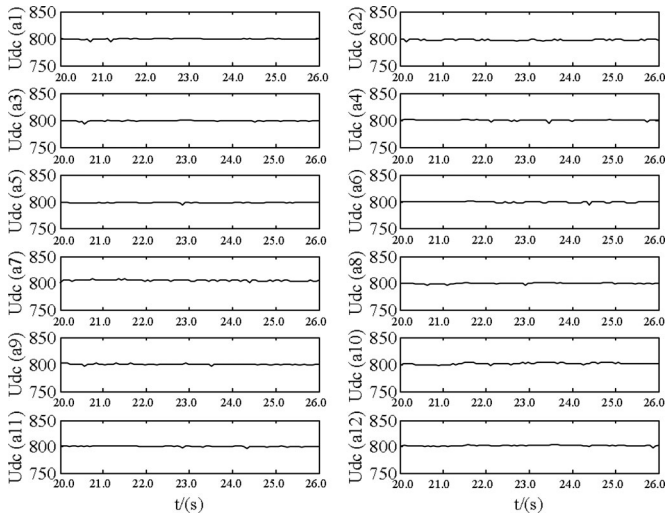


Fig. 17. Experimental waveforms of 12 cells in a-phase cluster for testing individual balancing control in the steady-state process.

## VI. Future Work

The application of a new nonlinear control method based on PBC theory in current loop control coupled with the dc capacitor voltage balancing control techniques described in this paper has been shown to be very effective at improving the steady state and dynamic performance of H-bridge cascaded STATCOM, and making the realization of control methods in DSP and FPGA became easier. Furthermore, the future work will focus on studying the control method of H-bridge cascaded STATCOM under unbalanced and distorted grid voltage. It will make H-bridge cascaded STATCOM run steadily and keep the ideal reactive compensation effect under any conditions.

The difference between the unbalanced and distorted grid with the balanced and no distorted grid only lies in that the negative sequence component and the harmonic component exist in the unbalanced and distorted grid, but they do not appear in the balanced and no distorted grid. So, on basis of the research results in this paper, H-bridge cascaded STATCOM can still achieve the satisfactory performance under unbalanced and distorted grid voltage by adding the negative sequence component controller and the harmonic component controller in current loop control, and also the corresponding voltage controller for restraining the impact of the negative sequence component on dc capacitor voltage balancing control.

To achieve this objective, in further investigation, the authors will focus on the work of the following respects.

1) Under unbalanced voltage, in order to obtain the negative sequence phase angle, the existing PLL which only obtains the positive sequence phase angle in this paper needs to be improved for extracting the positive sequence synchronizing signal and the negative sequence synchronizing signal separately.
2) The negative sequence component reference signal and the harmonic component reference signal also need to be calculated separately.
3) According to the proposed nonlinear control method based on PBC theory in this paper, the negative sequence component controller and the harmonic component controller will be designed and added in current loop control.
4) In order to restrain the impact of the negative sequence component on clustered balancing control, we will use the method of the zero-sequence voltage injection according to the dc voltage deviation. Because zero-sequence voltage has different effects on three-phase compensation current, but the sum of these different effects is zero in one cycle. Based on the previous characteristic, this method can be used for clustered balancing control under unbalanced grid voltage. And the proposed ADRC in this paper will be still used to realize the method of the zero-sequence voltage injection.

In addition, the proposed method for individual balancing control in this paper is achieved in the stage of CPS-SPWM and the dc voltage of each cell is controlled independently. So, it does not need to consider the impact of the negative sequence component. This method will continue to be used in future work.

## APPENDIX

### I. DISSIPATION SYSTEM THEORY AND ENERGY STORAGE FUNCTION

Because passivity theory is an important component of the dissipation system theory, it is necessary to know the definition of the dissipation system to prove that H-bridge cascaded STATCOM is strictly passive. Moreover, the energy storage function of system should be selected properly.

Let us first recall the definition of the dissipation system. Then, we will introduce that how to select the energy storage function of the system in this paper.

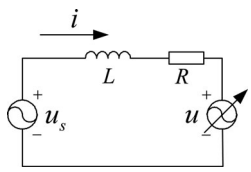


Fig. 18. a-phase cluster equivalent circuit of H-bridge cascaded STATCOM.

Dissipativity is the fundamental property of physical system closely related to energy losses and energy dissipation [54]. The typical example of energy dissipation system is circuit, in which partial electric energy and magnetic energy dissipate in the resistor in the form of heat. To accurately define dissipativity, it requires two functions: one reflects the rate of energy that flow into the system, namely supply rate; the other one is energy storage function that measure the system energy storage. These functions are connected by dissipative inequality. By "dissipative inequality," we mean that the supply rate is no less than the increment of energy storage along with the time track of the dissipation system. This means that the energy storage in the dissipation system should be no more than that of the external supply and the difference between the two numbers is the amount of dissipated energy.

Now, we introduce the dissipation system theory applied to H-bridge cascaded STATCOM. Consider a-phase cluster equivalent circuit of H-bridge cascaded STATCOM which is shown in Fig. 18.

According to the law of Kirchhoff, the dynamic equation of circuit can be obtained

$$L\frac{di}{dt} = u_s - u - Ri \tag{25}$$

where $u_s$ is the voltage of system. $u$ is the output voltage of STATCOM. $i$ is the output current of STATCOM. $L$ is the inductor. $R$ is the equivalent series resistance of the inductor.

By multiplying both sides of (25) by $i$, (26) is obtained as follows:

$$Li\frac{di}{dt} = (u_s - u)\, i - Ri^2. \tag{26}$$

Equation (26) can be equivalent to

$$\frac{d}{dt}\left(\frac{1}{2}Li^2\right) = (u_s - u)\, i - Ri^2 \tag{27}$$

where $\frac{1}{2}Li^2$ is the magnetic field energy which is stored in inductor, namely the storage energy of circuit.

Setting energy storage function $V = \frac{1}{2}Li^2$ and integrating (27) from 0 to $t$, (28) can be obtained

$$V(t) = V(0) + \int_0^t (u_s(\tau) - u(\tau))\, i(\tau)\, \mathrm{d}\tau - \int_0^t Ri^2(\tau)\mathrm{d}\tau \tag{28}$$

where $V(t)$ is the energy of circuit at $t$. $V(0)$ is initial energy of circuit. $\int_0^t (u_s(\tau) - u(\tau))\, i(\tau)\, \mathrm{d}\tau$ is the supplying energy of external power. $\int_0^t Ri^2(\tau)\mathrm{d}\tau$ is the dissipation energy of circuit. According to the definition of the dissipation system, H-bridge cascaded STATCOM is the dissipation system. Thus, basing on discusses in this paper, H-bridge cascaded STATCOM is the

strictly passive. Moreover, the selected energy storage function $V = \frac{1}{2}Li^2$ is appropriate.

Because the current is expressed in *d–q* axis in this paper, combining (4), the energy storage function can be written as the following form which is the same as (6):

$$V = \frac{1}{2}\mathbf{x}^{\mathrm{T}}\mathbf{M}\mathbf{x} = \frac{1}{2}L\left(i_d^2 + i_q^2\right). \tag{29}$$

## REFERENCES


[1] B. Gultekin and M. Ermis, "Cascaded multilevel converter-based transmission STATCOM: System design methodology and development of a 12 kV ±12 MVAr power stage," *IEEE Trans. Power Electron.*, vol. 28, no. 11, pp. 4930–4950, Nov. 2013.

[2] B. Gultekin, C. O. Gerçek, T. Atalik, M. Deniz, N. Biçer, M. Ermis, K. Kose, C. Ermis, E. Koç, I. Çadirci, A. Açik, Y. Akkaya, H. Toygar, and S. Bideci, "Design and implementation of a 154-kV±50-Mvar transmission STATCOM based on 21-level cascaded multilevel converter," *IEEE Trans. Ind. Appl.*, vol. 48, no. 3, pp. 1030–1045, May/Jun. 2012.

[3] S. Kouro, M. Malinowski, K. Gopakumar, L. G. Franquelo, J. Pou, J. Rodriguez, B. Wu, M. A. Perez, and J. I. Leon, "Recent advances and industrial applications of multilevel converters," *IEEE Trans. Ind. Electron.*, vol. 57, no. 8, pp. 2553–2580, Aug. 2010.

[4] F. Z. Peng, J.-S. Lai, J. W. McKeever, and J. VanCoevering, "A multilevel voltage-source inverter with separate DC sources for static var generation," *IEEE Trans. Ind. Appl.*, vol. 32, no. 5, pp. 1130–1138, Sep./Oct. 1996.

[5] Y. S. Lai and F. S. Shyu, "Topology for hybrid multilevel inverter," *Proc. Inst. Elect. Eng.—Elect. Power Appl.*, vol. 149, no. 6, pp. 449–458, Nov. 2002.

[6] D. Soto and T. C. Green, "A comparison of high-power converter topologies for the implementation of FACTS controllers," *IEEE Trans. Ind. Electron.*, vol. 49, no. 5, pp. 1072–1080, Oct. 2002.

[7] C. K. Lee, J. S. K. Leung, S. Y. R. Hui, and H. S.-H. Chung, "Circuit-level comparison of STATCOM technologies," *IEEE Trans. Power Electron.*, vol. 18, no. 4, pp. 1084–1092, Jul. 2003.

[8] H. Akagi, S. Inoue, and T. Yoshii, "Control and performance of a transformerless cascade PWM STATCOM with star configuration," *IEEE Trans. Ind. Appl.*, vol. 43, no. 4, pp. 1041–1049, Jul./Aug. 2007.

[9] A. H. Norouzi and A. M. Sharaf, "Two control scheme to enhance the dynamic performance of the STATCOM and SSSC," *IEEE Trans. Power Del.*, vol. 20, no. 1, pp. 435–442, Jan. 2005.

[10] C. Schauder, M. Gernhardt, E. Stacey, T. Lemak, L. Gyugyi, T. W. Cease, and A. Edris, "Operation of ±100 MVAr TVA STATCOM," *IEEE Trans. Power Del.*, vol. 12, no. 4, pp. 1805–1822, Oct. 1997.

[11] C. H. Liu and Y. Y. Hsu, "Design of a self-tuning PI controller for a STATCOM using particle swarm optimization," *IEEE Trans. Ind. Electron.*, vol. 57, no. 2, pp. 702–715, Feb. 2010.

[12] S. Mohagheghi, Y. Del Valle, G. K. Venayagamoorthy, and R. G. Harley, "A proportional-integrator type adaptive critic design-based neurocontroller for a static compensator in a multimachine power system," *IEEE Trans. Ind. Electron.*, vol. 54, no. 1, pp. 86–96, Feb. 2007.

[13] H. F. Wang, H. Li, and H. Chen, "Application of cell immune response modelling to power system voltage control by STATCOM," *Proc. Inst. Elect. Eng. Gener. Transm. Distrib.*, vol. 149, no. 1, pp. 102–107, Jan. 2002.

[14] A. Jain, K. Joshi, A. Behal, and N. Mohan, "Voltage regulation with STATCOMs: Modeling, control and results," *IEEE Trans. Power Del.*, vol. 21, no. 2, pp. 726–735, Apr. 2006.

[15] V. Spitsa, A. Alexandrovitz, and E. Zeheb, "Design of a robust state feedback controller for a STATCOM using a zero set concept," *IEEE Trans. Power Del.*, vol. 25, no. 1, pp. 456–467, Jan. 2010.

[16] C. D. Townsend, T. J. Summers, and R. E. Betz, "Multigoal heuristic model predictive control technique applied to a cascaded H-bridge STATCOM," *IEEE Trans. Power Electron.*, vol. 27, no. 3, pp. 1191–1200, Mar. 2012.

[17] C. D. Townsend, T. J. Summers, J. Vodden, A. J. Watson, R. E. Betz, and J. C. Clare, "Optimization of switching losses and capacitor voltage ripple using model predictive control of a cascaded H-bridge multilevel STATCOM," *IEEE Trans. Power Electron.*, vol. 28, no. 7, pp. 3077–3087, Jul. 2013.

[18] Y. Shi, B. Liu, and S. Duan, "Eliminating DC current injection in current-transformer-sensed STATCOMs," *IEEE Trans. Power Electron.*, vol. 28, no. 8, pp. 3760–3767, Aug. 2013.

[19] B. Singh and S. R. Arya, "Adaptive theory-based improved linear sinusoidal tracer control algorithm for DSTATCOM," *IEEE Trans. Power Electron.*, vol. 28, no. 8, pp. 3768–3778, Aug. 2013.

[20] S. R. Arya and B. Singh, "Performance of DSTATCOM using leaky LMS control algorithm," *IEEE J. Emerging Select. Topics Power Electron.*, vol. 1, no. 2, pp. 104–113, Jun. 2013.

[21] P. Petitclair, S. Bacha, and J.-P. Fe rrieux, "Optimized linearization via feedback control law for a STATCOM," in *Proc. IEEE Ind. Appl. Soc. Annu. Meeting*, 1997, pp. 880–885.

[22] H. Khalil, *Nonlinear Systems*, 3rd ed. Englewood Cliffs, NJ, USA: Prentice-Hall, 2002.

[23] Y. Han, Y. O. Lee, and C. C. Chung, "Modified non-linear damping of internal dynamics via feedback linearisation for static synchronous compensator," *IET Gener. Transm. Distrib.*, vol. 5, no. 9, pp. 930–940, 2011.

[24] Y. O. Lee, Y. Han, and C. C. Chung, "Output tracking control with enhanced damping of internal dynamics and its output boundedness for STATCOM system," *IET Control Theory Appl.*, vol. 6, no. 10, pp. 1445–1455, 2012.

[25] Y. O. Lee, Y. Han, and C. C. Chung, "Output tracking control with enhanced damping of internal dynamics and its output boundedness," in *Proc. IEEE Conf. Decision Control*, 2010, pp. 3964–3971.

[26] Y. Han, Y. O. Lee, and C. C. Chung, "A modified nonlinear damping of zero-dynamics via feedback control for a STATCOM," in *Proc. IEEE PowerTech*, 2009, pp. 880–885.

[27] G. E. Valderrama, P. Mattavelli, and A. M. Stankovic, "Reactive power and imbalance compensation using STATCOM with dissipativity-based control," *IEEE Trans. Control Syst. Technol.*, vol. 9, no. 5, pp. 718–727, Sep. 2001.

[28] H. Tsai, C. Chu, and S. Lee, "Passivity-based nonlinear STATCOM controller design for improving transient stability of power systems," presented at the IEEE/PES Transmission and Distribution Conference & Exhibition: Asia and Pacific, Dalian, China, 2005.

[29] Y. Gui, Y. O. Lee, H. J. Kang, Y. Han, and C. C. Chung, "Novel passivity-based controller design for STATCOM," in presented at the 2011 11th International Conference on Control, Automation and Systems, Gyeonggido, Korea, Oct. 26–29, 2011, pp. 556–560.

[30] Y. Gui, Y. O. Lee, Y. Han, W. Kim, and C. C. Chung, "Passivity-based control with nonlinear damping for STATCOM system," in *Proc. 51st IEEE Conf. Decision Control*, Maui, HI, Dec. 10–13, 2012, pp. 3964–3971.

[31] F. Z. Peng, W. S. John, and D. A. Adams, "A power line conditioner using cascade multilevel inverters for distribution systems," *IEEE Trans. Ind. Appl.*, vol. 34, no. 6, pp. 1293–1298, Nov./Dec. 1998.

[32] W. Jun and K. M. Smedley, "Synthesis of multilevel converters based on single- and/or three-phase converter building blocks," *IEEE Trans. Power Electron.*, vol. 23, no. 3, pp. 1247–1256, May 2008.

[33] C. H. Ng, M. A. Parker, R. Li, P. J. Tavner, J. R. Bumby, and E. Spooner, "A multilevel modular converter for a large, light weight wind turbine generator," *IEEE Trans. Power Electron.*, vol. 23, no. 3, pp. 1062–1074, May 2008.

[34] J. Geng, "Modeling and controlling of cascade static synchronous compensator," Ph.D. dissertation, Dept. Electr. Eng., Tsinghua Univ., Beijing, China, 2003.

[35] R. E. Betz and T. J. Summers, "Using a cascaded H-bridge STATCOM for rebalancing unbalanced voltages," presented at the 7th International Conference on Power Electronics, Daegu, Korea, Oct. 2007.

[36] N. Hatano and T. Ise, "A configuration and control method of cascade H-bridge STATCOM," presented at the IEEE Power Energy Society General Meeting, Pittsburgh, PA, USA, Jul. 2008.

[37] T. Yoshii, S. Inoue, and H. Akagi, "Control and performance of a medium-voltage transformerless cascade PWM STATCOM with star configuration," presented at the IEEE Industry Applications Conference, Tampa, FL, USA, 2006.

[38] M. Hagiwara and H. Akagi, "Control and experiment of pulse width modulated modular multilevel converters," *IEEE Trans. Power Electron.*, vol. 24, no. 7, pp. 1737–1746, Jul. 2009.

[39] Z. Liu, B. Y. Liu, S. X. Duan, and Y. Kang, "A novel DC capacitor voltage balance control method for cascade multilevel STATCOM," *IEEE Trans. Power Electron.*, vol. 27, no. 1, pp. 14–27, Jan. 2012.

[40] L. M. Tolbert, J. N. Chiasson, and F. Z. Peng, "Modulation index regulation of a multilevel inverter for static var compensation," in presented at the Power Engineering Society General Meeting, Toronto, ON, Canada, 2003, p. 199.

[41] Q. Song, W. Liu, Z. Yuan, W. Wei, and Y. Chen, "DC voltage balancing technique using multi-pulse optimal PWM for cascade H-bridge inverters based STATCOM," in *Proc. IEEE 35th Annu. Power Electron. Spec. Conf.*, Aachen, Germany, Jun. 20–25, 2004, pp. 4768–4772.
[42] Q. Song, W. Liu, Z. Yuan, W. Wei, and Y. Chen, "DC voltage balancing technique using multi-pulse optimal PWM for cascade H-bridge inverters based STATCOM," in *Proc. Appl. Power Electron. Conf. Expo.*, Anaheim, CA, 2004, pp. 4768–4772.
[43] Y. Li and B. Wu, "A novel DC voltage detection technique in the CHB inverter-based STATCOM," *IEEE Trans. Power Del.*, vol. 23, no. 3, pp. 1613–1619, Jul. 2008.
[44] S. Sirisukprasert, A. Q. Huang, and J.-S. Lai, "Modeling, analysis and control of cascaded-multilevel converter-based STATCOM," presented at the IEEE Power Engineering Society General Meeting, Toronto, ON, Canada, Jul. 2003.
[45] J. A. Barrena, L. Marroyo, M. A. Rodriguez, O. Alonso, and J. R. Torrealday, "DC voltage balancing for PWM cascaded H-bridge converter based STATCOM," in *Proc. 32nd Annu. Conf. Ind. Electron.*, Paris, France, 2006, pp. 1840–1845.
[46] J. A. Barrena, L. Marroyo, M. A. R. Vidal, and J. R. T. Apraiz, "Individual voltage balancing strategy for PWM cascaded H-bridge converter based STATCOM," *IEEE Trans. Ind. Electron.*, vol. 55, no. 1, pp. 21–29, Jan. 2008.
[47] K. Sano and M. Takasaki, "A transformerless D-STATCOM based on a multivoltage cascade converter requiring no DC sources," *IEEE Trans. Power Electron.*, vol. 27, no. 6, pp. 2783–2795, Jun. 2012.
[48] S. Du, J. Liu, J. Lin, and Y. He, "A novel DC voltage control method for STATCOM based on hybrid multilevel H-bridge converter," *IEEE Trans. Power Electron.*, vol. 28, no. 1, pp. 101–111, Jan. 2013.
[49] J. Q. Han, "Auto-disturbance rejection control and applications," *Control Decision*, vol. 13, pp. 19–23, 1998.
[50] J. Q. Han, "From PID to active disturbance rejection control," *IEEE Trans. Ind. Electron.*, vol. 56, no. 3, pp. 900–906, Mar. 2009.
[51] D. Wu, "Design and analysis of precision active disturbance rejection control for noncircular turning process," *IEEE Trans. Ind. Electron.*, vol. 56, no. 7, pp. 2746–2753, Jul. 2009.
[52] Q. Zheng, L. L. Dong, and Z. Gao, "Control and rotation rate estimation of vibrational MEMS gyroscopes," in *Proc. IEEE Int. Conf. Control Appl.*, Piscataway, NJ, 2007, pp. 118–123.
[53] W. Zhou and Z. Gao, "An active disturbance rejection approach to tension and velocity regulations in web processing lines," in *Proc. IEEE Int. Conf. Control Appl.*, Piscataway, NJ, 2007, pp. 842–848.
[54] R. Ortega, A. Loria, P. J. Nicklasson, and H. Sira-Ramirez, *Passivity-Based Control of Euler-Lagrange Systems: Mechanical Electrical and Electromechanical Application*. London, U.K.: Springer-Verlag, 1998.
[55] L. Maharjan, S. Inoue, and H. Akagi, "A transformerless energy storage system based on a cascade multilevel PWM converter with star configuration," *IEEE Trans. Ind. Appl.*, vol. 44, no. 5, pp. 1621–1630, Sep./Oct. 2008.

**Rong Xu** was born in Jilin Province, China, in 1984. He received the B.S. degree in applied physics from the Harbin University of Science and Technology, Harbin, China, in 2007, and the M.S. degree in power machinery and engineering from the Harbin Institute of Technology, Harbin, in 2009, where he is currently working toward the Ph.D. degree in electrical engineering.

His research interests include high-power power electronics, multilevel converters, and power quality mitigation.

**Yong Yu** was born in Jilin Province, China, in 1974. He received the B.S. degree in electromagnetic measurement and instrumentation from the Harbin Institute of Technology (HIT), where he also received the M.S. and Ph.D. degrees in electrical engineering in 1997 and 2003, respectively.

Since 2004, he has been an Associate Professor in the Department of Electrical Engineering, HIT. His current research interests include electrical motor drives, power quality mitigation, and fault diagnosis and tolerant control of inverter.

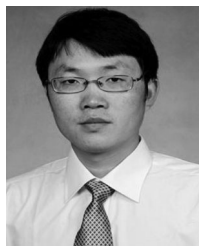

**Rongfeng Yang** received the B.S., Master, and Doctor degrees from Tsinghua University, Beijing, China, in 2001, 2003, and 2006, respectively, all in engineering physics.

In 2006, he joined the Department of Electrical Engineering, Harbin Institute of Technology, Harbin, China, as a Lecturer, where he finished postdoctoral work and his research interests was focused on sensorless induction motors control and high power medium voltage application.

**Gaolin Wang** (M'13) received the B.S., M.S., and Ph.D. degrees in electrical engineering from the Harbin Institute of Technology, Harbin, China, in 2002, 2004 and 2008, respectively.

In 2009, he joined the Department of Electrical Engineering, Harbin Institute of Technology as a Lecturer, where he has been an Associate Professor of Electrical Engineering since 2012. From 2009 to 2012, he was a Postdoctoral Fellow in Shanghai STEP Electric Corporation. He has authored more than 30 technical papers published in journals and conference proceedings. He is the holder of seven Chinese patents. His current major research interests include permanent magnet synchronous motor drives, high performance direct-drive for traction system, position sensorless control of ac motors and efficiency optimization control of interior PMSM.

**Dianguo Xu** (M'97–SM'12) received the B.S. degree in control engineering from Harbin Engineering University, Harbin, China, in 1982, and the M.S. and Ph.D. degrees in electrical engineering from the Harbin Institute of Technology (HIT), Harbin, in 1984 and 1989, respectively.

In 1984, he joined the Department of Electrical Engineering, HIT, as an Assistant Professor. Since 1994, he has been a Professor in the Department of Electrical Engineering, HIT. He was the Dean of School of Electrical Engineering and Automation, HIT, from 2000 to 2010. He is currently the Assistant President of HIT. His research interests include renewable energy generation technology, multiterminal HVDC system based on VSC, power quality mitigation, speed sensorless vector controlled motor drives, and high performance PMSM servo system. He has published more than 600 technical papers.

Dr. Xu is an Associate Editor for the IEEE TRANSACTIONS ON INDUSTRIAL ELECTRONICS. He serves as the Chairman of IEEE Harbin Section, Director of Lighting Power Supply Committee of CPSS, Vice-Director of Electric Automation Committee of CAA, Electrical Control System & Equipment Committee of CES, and Power Electronics Committee of CES.

**Binbin Li** was born in 1989. He received the B.S. and M.S. degrees in electrical engineering from the Harbin Institute of Technology, Harbin, China, in 2010 and 2012, respectively, where he is currently working toward the Ph.D. degree.

His research interests include high-power electronics, multilevel converters, control algorithms, and pulse width modulation techniques.

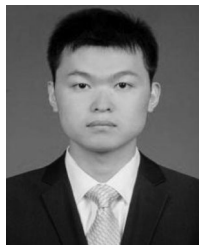

**Shunke Sui** was born in 1989. He received the B.S. degree in electrical engineering from the Chinese University of Mining and Technology, Beijing, China, and is currently working toward the M.S. degree at the Harbin Institute of Technology, Harbin, China.

His research interests include modular multilevel converter.